Electronic Supplementary Material (ESI) for Inorganic Chemistry Frontiers.

In-situ growth of MOF-derived nitrogen-doped carbon nanotubes on hollow MXene spheres for K-ion storage

Xiaoyu Chen, Shuanghong Xia, Tianyu Tan, Yajing Zhu, Ling Li*, Qiancheng Zhu*, Wenming Zhang*

Province-Ministry Co-construction Collaborative Innovation Center of Hebei Photovoltaic Technology, College of Physics Science and Technology, Hebei University, Baoding, Hebei 071002, China

Corresponding author at:

E-mail: lilinghbu@163.com (L. Li), whqianchengzhu@163.com (Q Zhu), wmzhanghbu@126.com (W. Zhang)

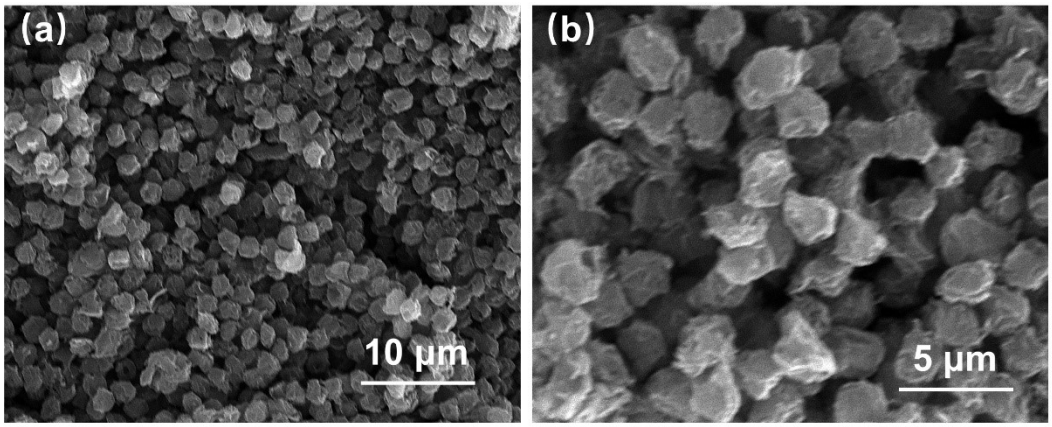

Figure S1 Scanning electron microscopy (SEM) images of SMXene.

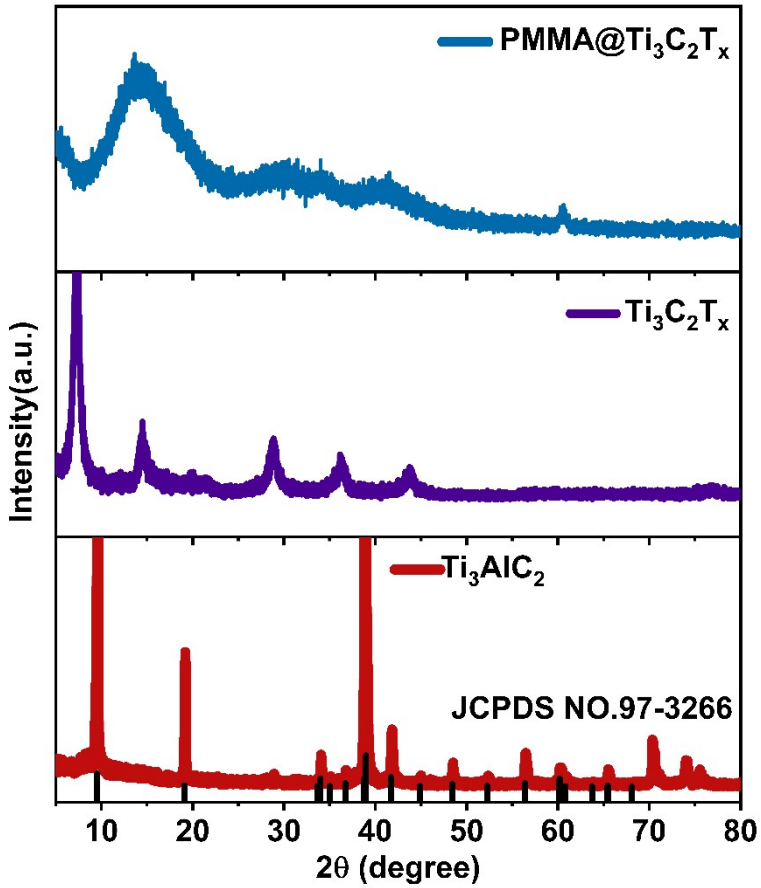

Figure S2 XRD patterns of Ti_3AlT_x, $Ti_3C_2T_x$, and PMMA@$Ti_3C_2T_x$.

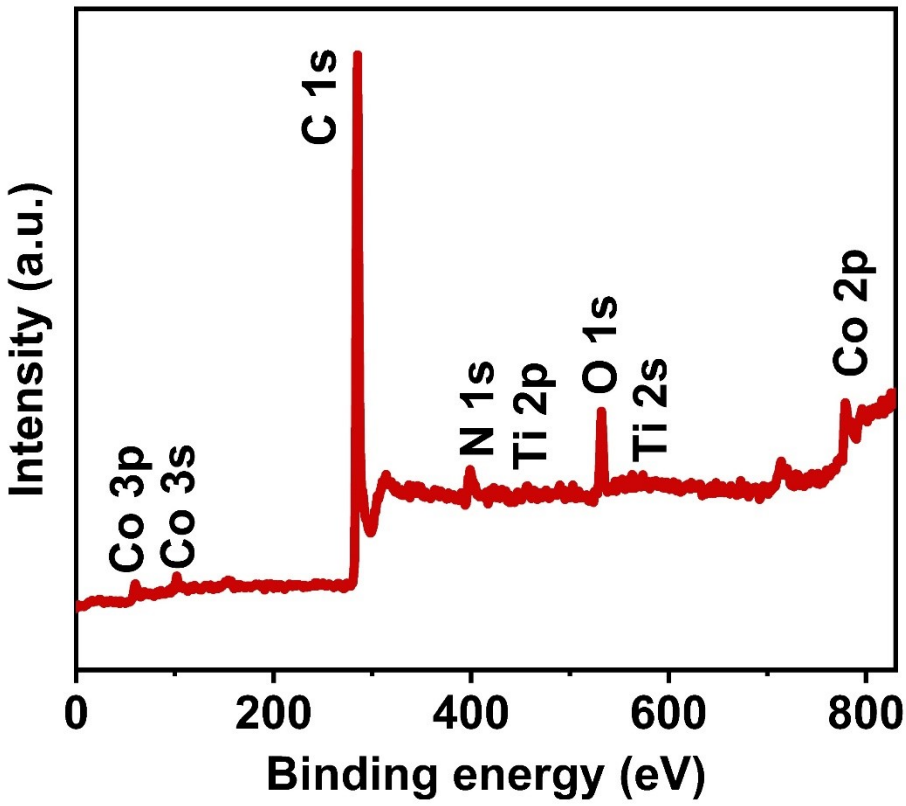

Figure S3 XPS spectra of CoN-CNT@SMXene.

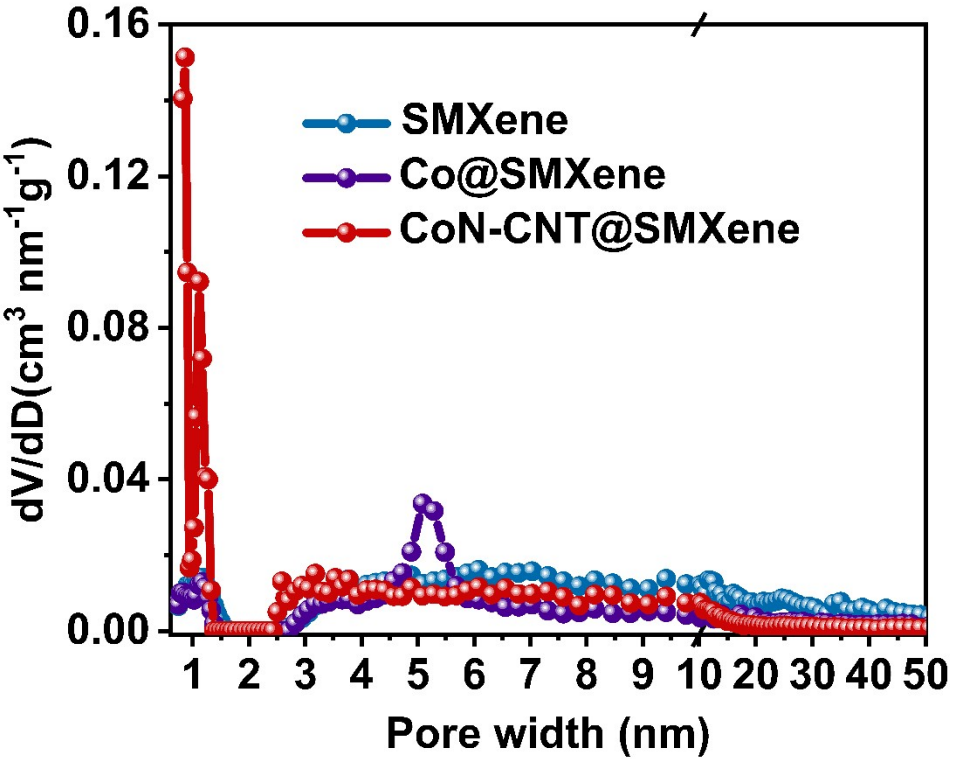

Figure S4 The pore size distribution curves obtained by DFT method.

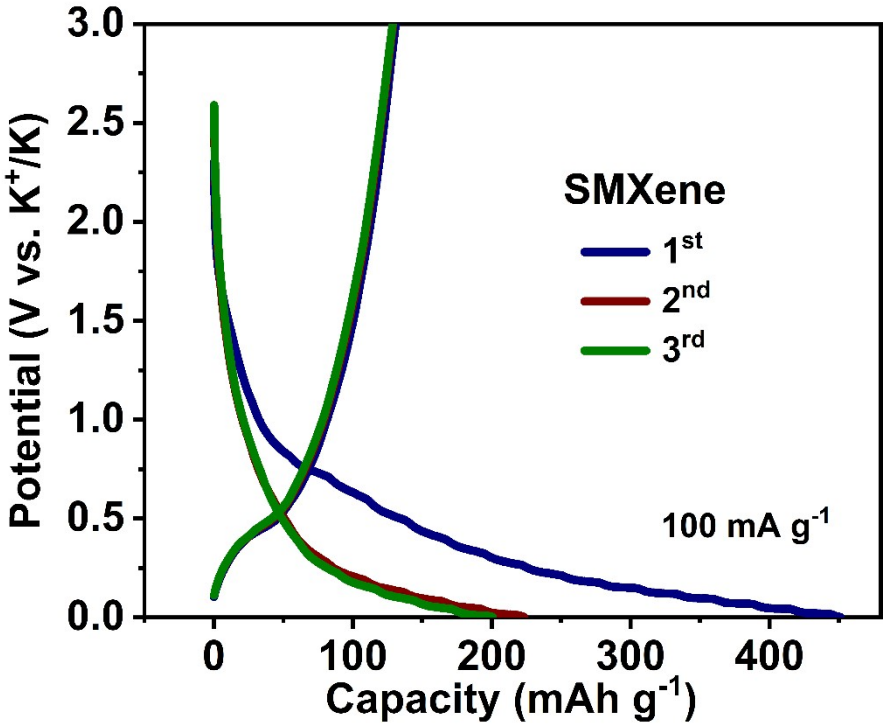

Figure S5 Discharge–charge profiles of SMXene at 0.1 A g^{-1} at different cycles.

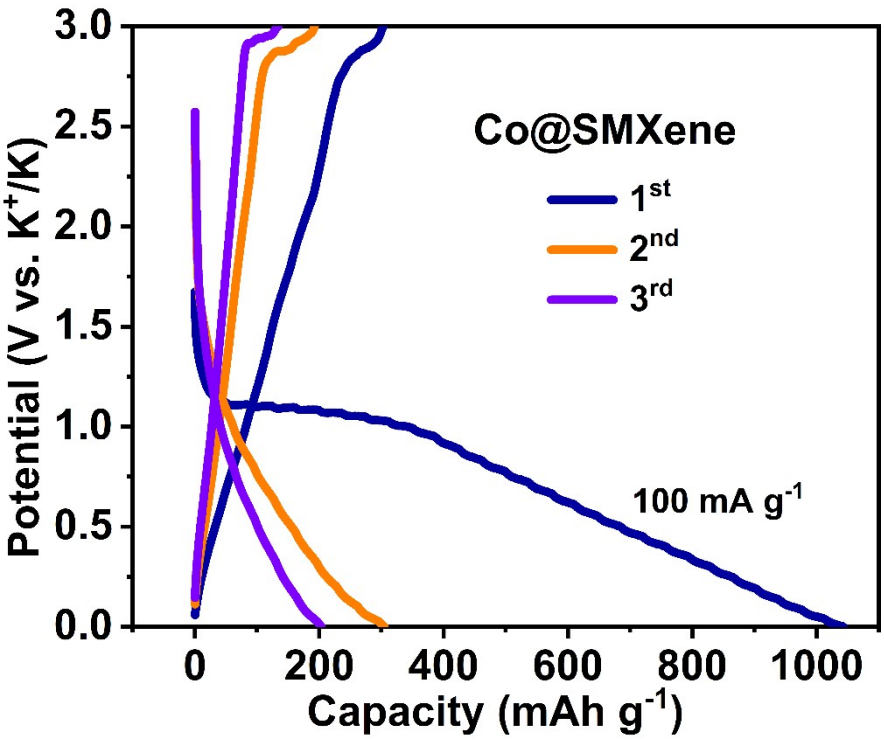

Figure S6 Discharge–charge profiles of Co@SMXene at 0.1 A g^{-1} at different cycles.

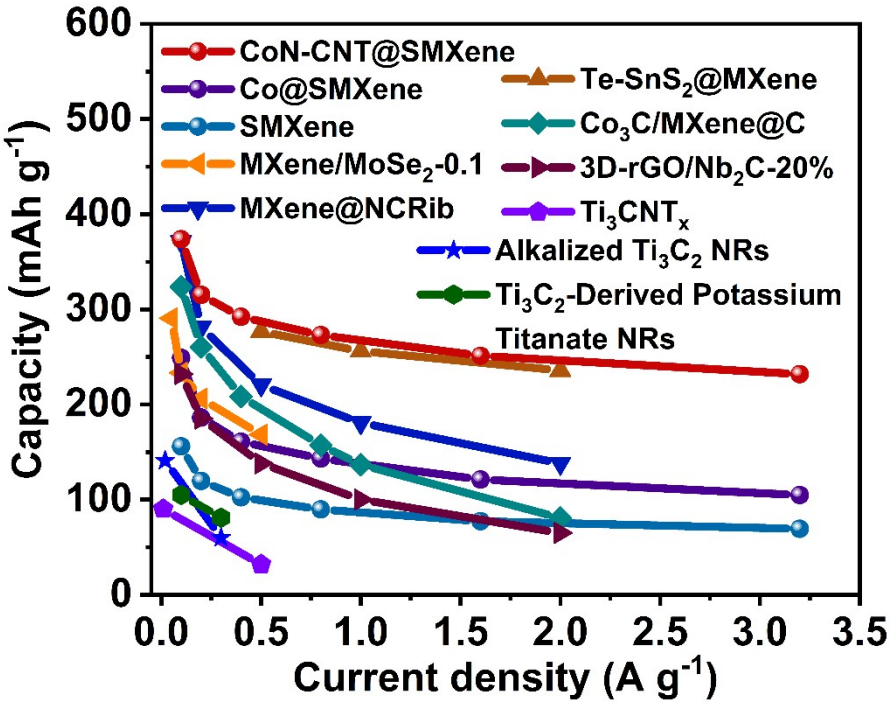

Figure S7 Comparison of rate capability with the reported work.

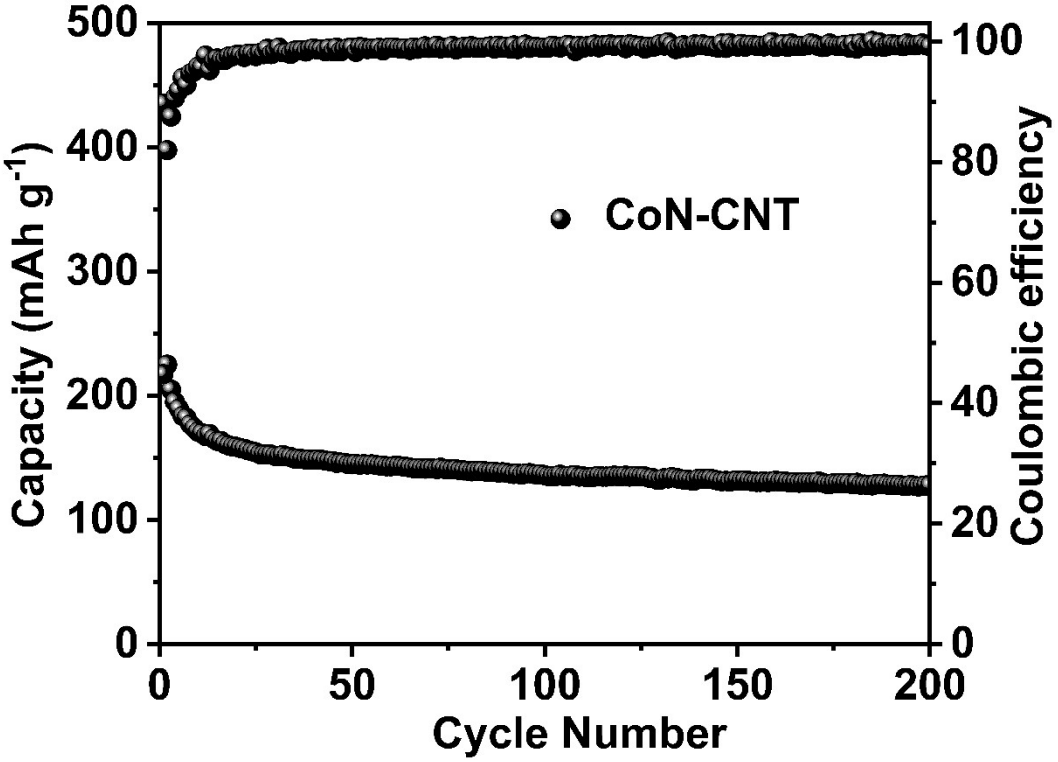

Figure S8 Cycling performance of CoN-CNT electrodes at 0.1 A g^{-1} for 200 cycles.

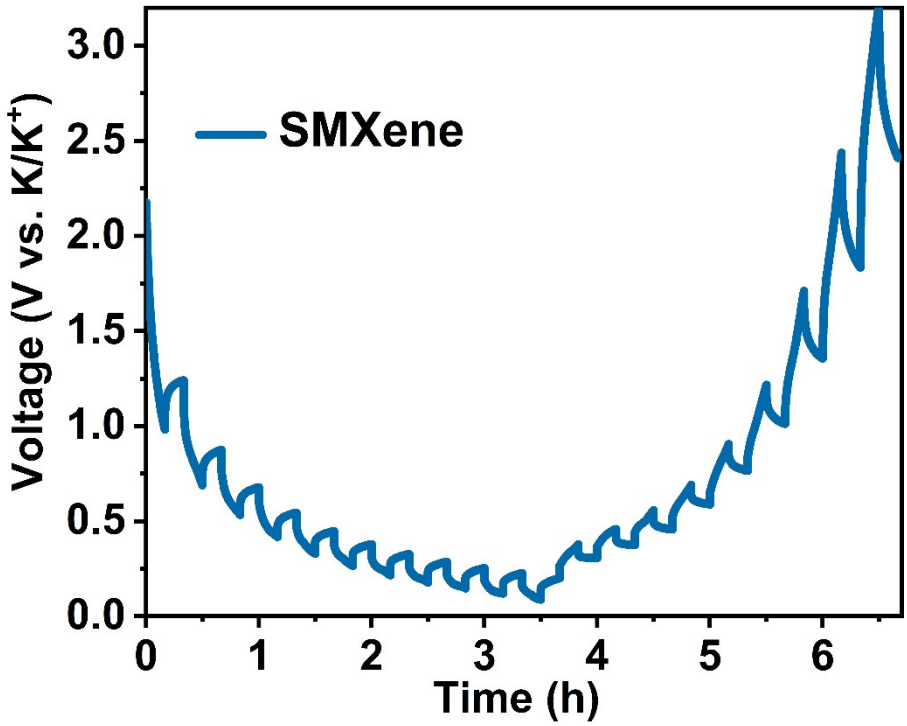

Figure S9 GITT potential profiles for SMXene.

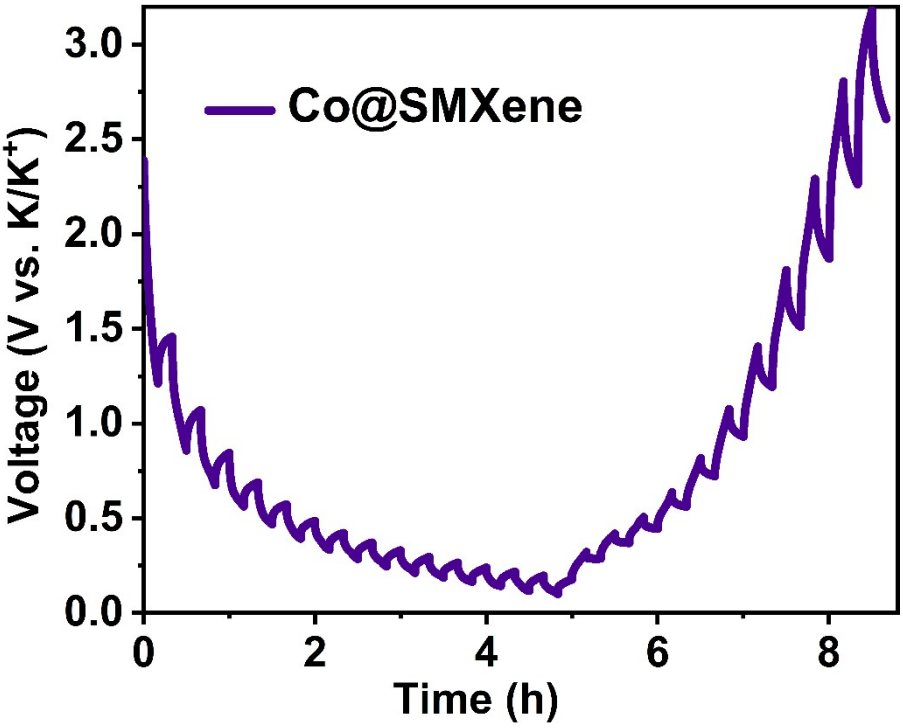

Figure S10 GITT potential profiles for Co@SMXene.

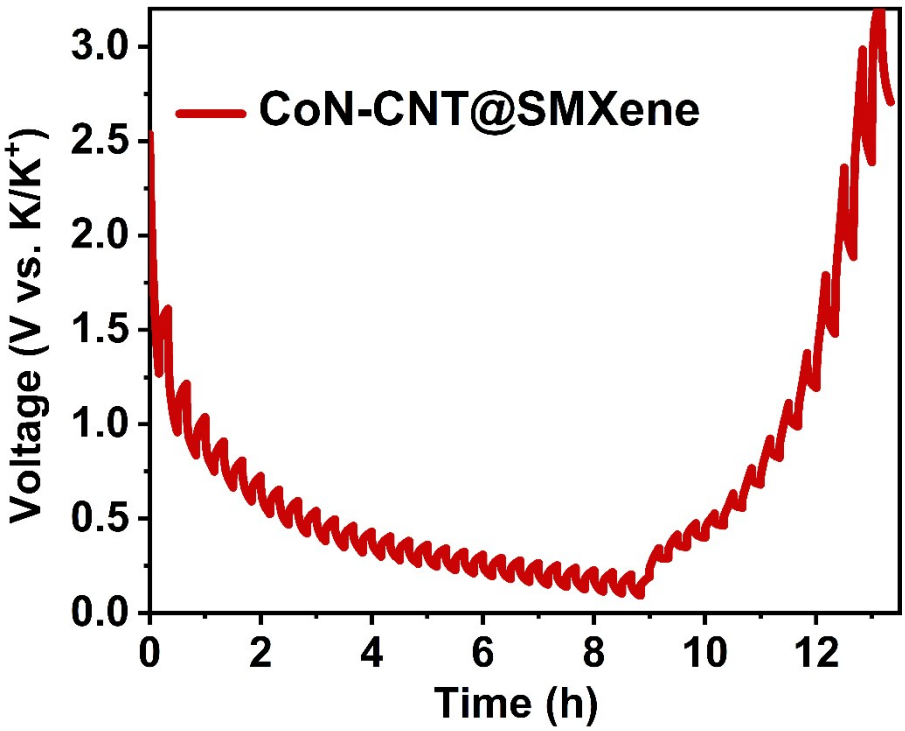

Figure S11 GITT potential profiles for Co-CNT@SMXene.

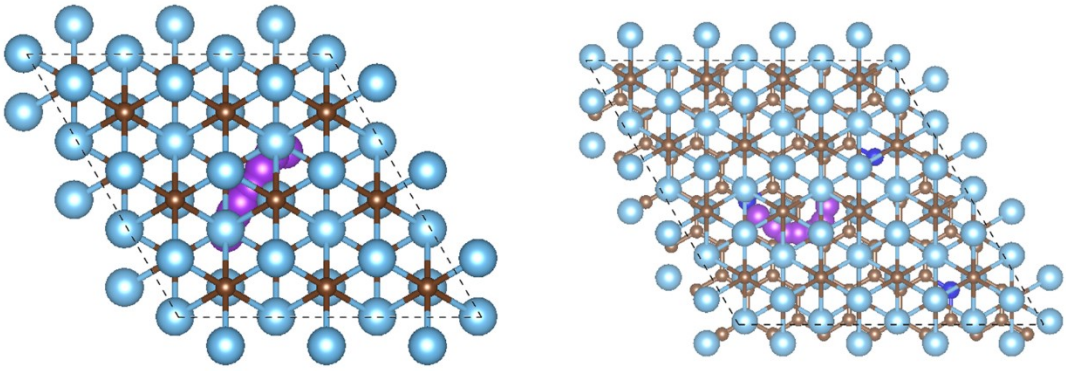

Figure S12 The migration path of K^+ in Ti_3C_2 and Ti_3C_2/CN.

Table S1 The detailed determination of cobalt, titanium, carbon and nitrogen calculated by means of ICP-MS and EA methods for the CoN-CNT@SMXene.

Methods	Sample weight (mg)	Co (g/kg)	Ti (g/kg)	C (%)	N (%)
ICP-MS	0.0132	49.8945	6.5936	-	-
EA	1.27	-	-	56.7608	37.5904

Table S2 The specific surface area.

	SMXene	Co@SMXene	CoN-CNT@SMXene
BET Surface area	153.4 $m^2 g^{-1}$	91.6 $m^2 g^{-1}$	253.8 $m^2 g^{-1}$
DFT pore size	6.079 nm	5.086 nm	0.863 nm

Table S3 Comparison of performances of MXene-based materials in PIBs.

Materials	Current density (mA g^{-1})	Capacity (mAh g^{-1})	Ref.
CoN-CNT@SMXene	100	373.6	This work
MXene/$MoSe_2$-0.1	100	233.1	Ref. 1
MXene@NCRib	200	281.4	Ref. 2
Te-SnS_2@MXene	500	276.7	Ref. 3
Co_3C/MXene@C	100	323.7	Ref. 4
Ti_3CNT_x	500	32	Ref. 5
Alkalized Ti_3C_2 NRs	300	60	Ref. 6
Ti_3C_2-Derived Potassium Titanate NRs	100	105	Ref. 7

Table S4 Comparison of performances of anode materials in PIBs.

Materials	Current density (mA g^{-1})	Capacity (mAh g^{-1})	Ref.
CoN-CNT@SMXene	100	373.6	This work
$K_2V_3O_8$	100	242	Ref. 8
N-doped hierarchical porous carbon	100	263.6	Ref. 9
Porous carbon microspheres	100	264.5	Ref. 10
Bi_2O_3@C	500	233	Ref. 11
ZnS@C	100	270	Ref. 12
$Bi_2Sn_2O_7$/C	50	295	Ref. 13

References

[1] J. Li, B. Rui, W. Wei, P. Nie, L. Chang, Z. Le, M. Liu, H. Wang, L. Wang, X. Zhang, Nanosheets assembled layered MoS_2/MXene as high performance anode materials for potassium ion batteries, *Journal of Power Sources*, 2020, **449**, 227481.

[2] J. Cao, Z. Sun, J. Li, Y. Zhu, Z. Yuan, Y. Zhang, D. Li, L. Wang, W. Han, Microbe-Assisted assembly of $Ti_3C_2T_x$ MXene on fungi-derived nanoribbon heterostructures for ultrastable sodium and potassium ion storage, *ACS nano*, 2021,**15**, 3423-3433.

[3] H. Sun, Y. Zhang, X. Xu, J. Zhou, F. Yang, H. Li, H. Chen, Y. Chen, Z. Liu, Z. Qiu, D. Wang, L. Ma, J. Wang, Q. Zeng, Z. Peng, Strongly coupled Te-SnS_2/MXene superstructure with self-autoadjustable function for fast and stable potassium ion storage, *Journal of Energy Chemistry,* 2021, **61**, 416-424.

[4] H. Zhang, D. Xiong, Y. Xie, K. Wu, Z. Feng, K. Wen, Z. Li, M. He, Co_3C/Mxene composites wrapped in N-rich carbon as stable-performance anodes for potassium/sodium-ion batteries, *Colloids and Surfaces A: Physicochemical and Engineering Aspects*, 2023, **656**, 130332.

[5] M. Naguib, R. A. Adams, Y. Zhao, D. Zemlyanov, A. Varma, J. Nanda, V. G. Pol, Electrochemical performance of MXenes as K-ion battery anodes, *Chemical Communications,* 2017, **53**, 6883-6886.

[6] P. Lian, Y. Dong, Z-S. Wu, S. Zheng, X. Wang, S. Wang, C. Sun, J. Qin, X. Shi, X. Bao, Alkalized Ti_3C_2 MXene nanoribbons with expanded interlayer spacing for high-capacity sodium and potassium ion batteries, *Nano Energy*, 2017, **40**, 1-8.

[7] Y. Dong, Z-S. Wu, S. Zheng, X. Wang, J. Qin, S. Wang, X. Shi, X. Bao, Ti_3C_2

MXene-derived sodium/potassium titanate nanoribbons for high-performance sodium/potassium ion batteries with enhanced capacities *ACS nano*, 2017, **11**, 4792-4800.

[8] M. Lu, K. Wang, H. Ke, Q. Hu, Z. Liu and H. Wu, Potassium vanadate $K_2V_3O_8$ as a superior anode material for potassium-ion batteries, *Mater. Lett.* 2018, **232**, 224-227.

[9] C. Gao, Q. Wang, S. Luo, Z. Wang, Y. Zhang, Y. Liu, A. Hao and R. Guo, High performance potassium-ion battery anode based on biomorphic N-doped carbon derived from walnut septum, *J. Power Sources*, 2019, **415**, 165-171.

[10] S. Chen, K. Tang, F. Song, Z. Liu, N. Zhang, S. Lan, X. Xie and Z. Wu, Porous hard carbon spheres derived from biomass for high-performance sodium/potassium-ion batteries, *Nanotechnology*, 2022, **33**, 055401.

[11] H. Tong, S. Chen, J. Tu, X. Zeng, C. Wang, P. Wang and Q. Chen, Bi_2O_3 particles embedded in carbon matrix as high-performance anode materials for potassium ion batteries, *J. Power Sources*, 2022, **549**, 232140.

[12] Y. Gan, M. Mu, M. Li, X. Ma, J. Yuan, H. He, X. Li, J. Mou, C. Zhang, X. Zhang and J. Liu, Trumpet-like ZnS@C composite for high-performance potassium ion battery anode, *Chem-Eur J.* 2023, DOI: 10.1002/chem.202300373.

[13] V. Ahuja, S. Baskar and P. Senguttuvan, Exploration of pyrochlore-$Bi_2Sn_2O_7$ as an anode for potassium-ion batteries, *ACS Appl. Energy Mater.* 2023, **6**, 3665–3670.